Contributions of Long-Range Electrostatic Interactions to 4-Chlorobenzoyl-CoA Dehalogenase Catalysis: A Combined Theoretical and Experimental Study†

Jingbo Wu, Dingguo Xu, Xuefeng Lu, Canhui Wang, Hua Guo,* and Debra Dunaway-Mariano*

Department of Chemistry, University of New Mexico, Albuquerque, New Mexico 87131

Received July 26, 2005; Revised Manuscript Received October 17, 2005

ABSTRACT: It is well established that electrostatic interactions play a vital role in enzyme catalysis. In this work, we report theory-guided mutation experiments that identified strong electrostatic contributions of a remote residue, namely, Glu232 located on the adjacent subunit, to 4-chlorobenzoyl-CoA dehalogenase catalysis. The Glu232Asp mutant was found to bind the substrate analogue 4-methylbenzoyl-CoA more tightly than does the wild-type dehalogenase. In contrast, the k_{cat} for 4-chlorobenzoyl-CoA conversion to product was reduced 10000-fold in the mutant. UV difference spectra measured for the respective enzyme−ligand complexes revealed an ∼3-fold shift in the equilibrium of the two active site conformers away from that inducing strong π-electron polarization in the ligand benzoyl ring. Increased substrate binding, decreased ring polarization, and decreased catalytic efficiency indicated that the repositioning of the point charge in the Glu232Asp mutant might affect the orientation of the Asp145 carboxylate with respect to the substrate aromatic ring. The time course for formation and reaction of the arylated enzyme intermediate during a single turnover was measured for wild-type and Glu232Asp mutant dehalogenases. The accumulation of arylated enzyme in the wild-type dehalogenase was not observed in the mutant. This indicates that the reduced turnover rate in the mutant is the result of a slow arylation of Asp145, owing to decreased efficiency in substrate nucleophilic attack by Asp145. To rationalize the experimental observations, a theoretical model is proposed, which computes the potential of mean force for the nucleophilic aromatic substitution step using a hybrid quantum mechanical/molecular mechanical method. To this end, the removal or reorientation of the side chain charge of residue 232, modeled respectively by the Glu232Gln and Glu232Asp mutants, is shown to increase the rate-limiting energy barrier. The calculated 23.1 kcal/mol free energy barrier for formation of the Meisenheimer intermediate in the Glu232Asp mutant represents an increase of 6 kcal/mol relative to that of the wild-type enzyme, consistent with the 5.6 kcal/mol increase calculated from the difference in experimentally determined rate constants. On the basis of the combination of the experimental and theoretical evidence, we hypothesize that the Glu232(B) residue contributes to catalysis by providing an electrostatic force that acts on the Asp145 nucleophile.

The enzyme 4-chlorobenzoyl-CoA (4-CBA-CoA)[1] dehalogenase is found in 4-chlorobenzoate-degrading bacteria (*1*, *2*) wherein it catalyzes the hydrolytic dehalogenation of 4-chorobenzoyl-CoA (4-CBA-CoA). Because of the uniqueness of the nucleophilic aromatic substitution reaction catalyzed and the potential application of this enzyme in the bioremediation of halogenated aromatics (*3*, *4*), much effort has been devoted to understanding its catalytic mechanism (*5*−*22*). The dehalogenation reaction proceeds via two partial reactions: nucleophilic aromatic substitution (S_NAr) (*23*), followed by ester hydrolysis (Scheme 1). In the first partial reaction an active site residue (Asp145) attacks the C(4) position of the substrate benzoyl ring in the enzyme−substrate complex (ES) to form the enzyme−Meisenheimer complex (EMc). The expulsion of the chloride ion yields the arylated enzyme complex (EAr). This intermediate is then hydrolyzed by a His90-bound water molecule forming 4-hydroxylbenzoyl-CoA (4-HBA-CoA), which is subsequently released from the enzyme.

The high-resolution X-ray structure of wild-type dehalogenase complexed with 4-HBA-CoA (EP) has shown that the active site is formed at the subunit interface of the homotrimer (Figure 1A) (*24*). The substrate adopts a U-shaped conformation with the benzoyl moiety extending into a deep active site cavity, in close proximity of the Asp145 nucleophile. The benzoyl carbonyl oxygen is engaged in hydrogen bond interactions with the backbone amide NHs of Gly114 and Phe64 (Figure 1B) and electrostatic interaction with the positive pole of the active site α-helix (pictured in Figure 1A), which terminates in Gly114. Collectively, these interactions comprise what will be referred to hereafter as the "oxyanion hole". The oxyanion hole effect is amplified by the network of hydrogen bonds that extend from this site

† This work was supported by NIH Grant GM28688 to D.D.-M. and by NSF Grant MCB-0313743 to H.G.

* To whom correspondence should be addressed. D.D.-M.: tel, 505-277-3383; fax, 505-277-6202; e-mail, dd39@unm.edu. H.G.: tel, 505-277-1716; fax, 505-277-2609; e-mail, hguo@unm.edu.

[1] Abbreviations: 4-CBA, 4-chlorobenzoate; 4-CBA-CoA, 4-chlorobenzoyl-coenzyme A; 4-HBA, 4-hydroxybenzoate; 4-HBA-CoA, 4-hydroxybenzoyl-coenzyme A; 4-MBA-CoA, 4-methylbenzoyl-coenzyme A; ES, enzyme−substrate complex; EP, enzyme−product complex; EMc, enzyme−Meisenheimer complex; EAr, arylated enzyme complex; DTT, dithiothreitol; K^+Hepes, potassium salt of *N*-(2-hydroxyethyl)-piperazine-*N*′-2-ethanesulfonate; PMF, potential of mean force; GSD, ground state destabilization; NAC, near-attack conformation.

10.1021/bi051477w CCC: $33.50
Published on Web 12/06/2005

Scheme 1: Mechanism of 4-CBA-CoA Dehalogenase Catalysis

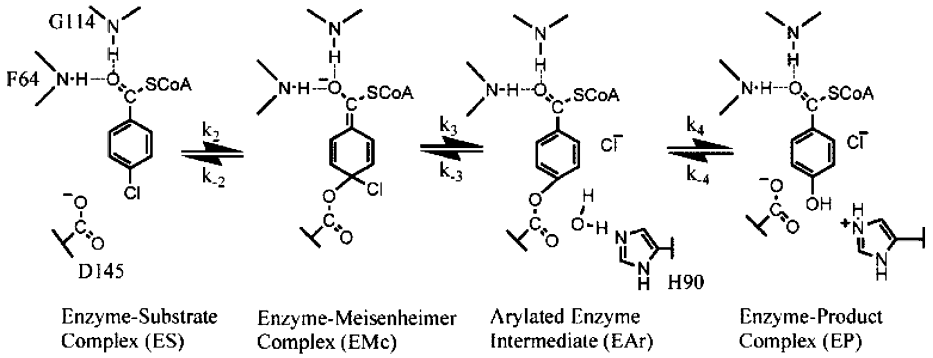

(*22*, *24*, *25*). The aromatic side chains that closely encircle the benzoyl ring (Figure 1B) might serve to enhance the π-electron pull effect of the oxyanion hole at one end of the benzoyl ring and the π-electron push effect of the Asp145 carboxyl anion directed at the opposite end of the ring (*11*). The degree of polarization of the benzoyl π-electrons, as

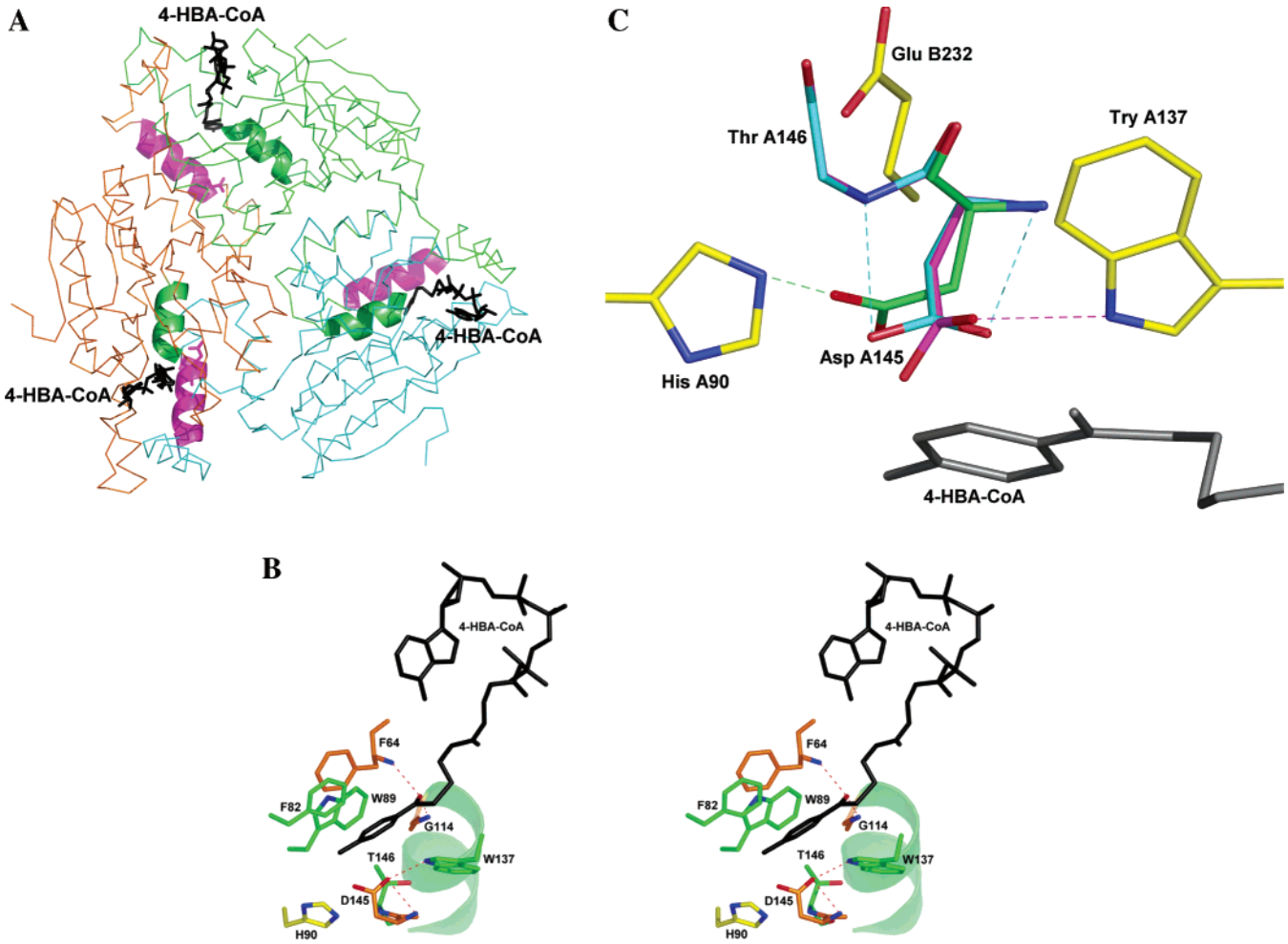

FIGURE 1: (A) Ribbon representation of the 4-CBA-CoA dehalogenase trimer generated from the X-ray coordinates of the wild-type 4-CBA-CoA dehalogenase−4-HBA-CoA complex (*24*). Chains A, B, and C are shown in green, orange, and cyan, respectively. 4-HBA-CoA is in black, the Glu232 α-helix is in magenta, and the Gly114 α-helix is in lime. (B) Active site of the 4-CBA-CoA dehalogenase−4-HBA-CoA complex (*24*). The ligand 4-HBA-CoA is shown in black. The side chains of the aromatic residues Phe64 (orange), Phe82 (green), Trp89 (green), and Trp137 (green) form the hydrophobic sheath. The Asp145 nucleophile is colored orange, the His90 base yellow, the H-bond donor Gly114 orange, the Thr146 green, and the α-helix green. Oxygen atoms are in red, and nitrogen atoms are in blue. Dashed lines signify hydrogen bonds. (C) Representation of three conformations of the Asp145 side chain. The side chain of Asp145 observed in the X-ray structure of the wild-type dehalogenase−4-HBA-CoA complex (*24*) is colored magenta. The side chain of Asp145 observed in the X-ray structure of the W137F dehalogenase−4-HBA-CoA and W137F dehalogenase−4-MBA-CoA complexes is colored lime (H. M. Holden and M. M. Benning, unpublished results). For the NAC conformation, the Asp145 side chain is colored cyan. To generate this conformation, the side chain of Asp145 was manually rotated from its position in the 4-HBA-CoA complex [viz. as in (B)] (*24*) to satisfy the conditions of the NAC conformation (*26*, *32*). The side chains of His90, Trp137, and Glu232(B), as observed in the X-ray crystal structure of the 4-CBA dehalogenase−4-HBA-CoA complex (*24*), are colored yellow, and the backbone of Thr146 is colored cyan. Dashed lines signify hydrogen bonds.

measured by Raman difference spectroscopy (*16*), has been correlated with the efficiency of EMc formation. The oxyanion hole binds the EMc more tightly than it does the substrate (*19*). In contrast, the Asp145 point charge appears to destabilize the ES complex (*16*). Specifically, replacement of Asp145 with a neutral amino acid increases the substrate binding affinity while it decreases the polarization of the benzoyl ring (*17*). Because the charge on the Asp145 residue dissipates into the entire benzoyl moiety as the transition state is reached, the electrostatic interaction might contribute to a reduction in the energy barrier.

Theoretical studies have indicated that the Asp145 side chain assumes a "near attack conformation" (NAC) prior to its attack at C(4) of the substrate ring (*26*, *27*). This conformation, which is stabilized by hydrogen bond interaction with the backbone amide of Thr146, differs from that observed in the crystal structure of the wild-type dehalogenase−4-HBA-CoA complex, which is stabilized by hydrogen bond interaction with the Trp137 indole NH, the Asp145 backbone NH, and the C(4)OH of the product ligand (Figure 1C) (*24*). It also differs from that observed in the crystal structure of the W137F dehalogenase−4-HBA-CoA complex, which is stabilized by hydrogen bond interaction with His90 (H. M. Holden and M. M. Benning, unpublished data). Although conformationally mobile, Asp145 exerts an electronic field effect on the π-electron density at the carbon that it will attack from its NAC.

As part of a combined theoretical−experimental approach to understanding dehalogenase catalysis, we have examined the hypothesis that orientation of the Asp145 nucleophile and/or the strength of its field effect is modulated by electrostatic interaction with residues located outside of the catalytic site. In this paper we focus on Glu232(B), positioned in an adjacent subunit (see the Glu232 side chain on the magenta helix in Figure 1A). The point charge of the Glu232(B) carboxylate is positioned ~6 Å from the Asp145 point charge (see Figure 1C). The Glu232(B) residue, as well the Arg216(B) which orients it, is stringently conserved among 4-CBA-CoA dehalogenase sequences. The potential contribution of the Glu232(B) residue to EMc formation was discovered in this study by a charge perturbation analysis and supported by subsequent computation of the QM/MM free energy profiles for the theoretical reaction coordinate of the E232D and E232Q dehalogenase mutants. The E232D dehalogenase mutant was then prepared and characterized to demonstrate increased substrate binding affinity, reduced benzoyl ring polarization, and reduced efficiency for catalysis of the S_NAr partial reaction. These findings, reported in the text that follows, are interpreted as evidence for a significant role of a preorganized dipole originating from the Arg216(B)−Glu232(B) ion pair located on one subunit in facilitating nucleophilic attack by Asp145 of the adjacent subunit (*28*, *29*) on the C(4) of the substrate 4-CBA-CoA benzoyl.

MATERIALS AND METHODS

Materials. 4-CBA-CoA, 4-MBA-CoA, 4-HBA-CoA, and wild-type dehalogenases were prepared according to published procedures (*7*).

Preparation of the E232D Dehalogenase. QuickChange mutagenesis (Stratagene) was used in combination with the *Sma*I−*Sal*IpT7.5 plasmid (containing the 4-CBA-CoA dehalogenase gene) as a template (*6*) and the *Escherichia coli* BL21(DE3) cell line for construction of site-directed mutants. Mutant sequences were confirmed by DNA sequencing. In total, 10 mutants were constructed: Glu232Ala, Glu232Gln, Glu232Asp, Glu232Asn, Glu232Arg, Arg216Leu, Arg216Lys, Arg216Glu, Glu232Gln/Arg216Leu, and Glu232Arg/Arg216Glu. The Glu232Asp mutant, the only soluble one, was purified as follows. A single colony of *E. coli* BL21(DE3) cells transformed with the mutant Glu232Asp dehalogenase-encoding plasmid was used to inoculate 10 mL of LB medium containing 50 μg/mL ampicillin at 37 °C and 250 rpm. The 10 mL culture was then used to inoculate 3 × 2 L of fresh LB medium containing 50 μg/mL ampicillin, and the culture was grown at 25 °C and 180 rpm for ~10 h (cell density had reached OD_{600} 0.6−0.8). After a 4 h induction period with 0.4 mM isopropyl β-D-galactopyranoside, the cells were harvested by centrifugation to yield ~13 g of wet cells. The cell pellet was suspended in 130 mL of buffer [50 mM K^+Hepes and 1 mM DTT (pH 7.5)] at 0 °C, passed through a French press at 1200 psi, and then centrifuged at 48000*g* and 4 °C for 0.5 h. The supernatant was loaded onto a 40 × 5 cm DEAE-Sepharose column [preequilibrated with 50 mM K^+Hepes and 1 mM DTT (pH 7.5)] at 4 °C, which was then washed with 1 L of 50 mM K^+Hepes/1 mM DTT (pH 7.5) before starting the 1.4 L linear gradient of 0−0.5 M KCl in 50 mM K^+Hepes/1 mM DTT (pH 7.5). The column fractions were analyzed by SDS−PAGE. The dehalogenase eluted at 0.35 M KCl. The desired protein fractions were combined and dialyzed in 50 mM K^+-Hepes/1 mM DTT (pH 7.5) for 2 × 1 h at 4 °C prior to loading onto a 18 cm × 3 cm hydroxyapatite column [preequilibrated with 50 mM K^+Hepes/1 mM DTT (pH 7.5)]. After washing with 300 mL of equilibration buffer, the column was eluted at 4 °C with a 600 mL linear gradient from 0 to 0.5 M K_2HPO_4 in 50 mM K^+Hepes/1 mM DTT (pH 7.5). The purified protein (eluted at ~0.2 M potassium phosphate) was concentrated using an Amicon device (10 kDa Disk membrane) or a 10 kDa Macrosep centricon. The protein purity was confirmed by SDS−PAGE. The protein concentration was determined by using the Bradford method (*30*) and by the protein absorbance at 280 nm (using the extinction coefficient of wild type: 40090 M^{-1} cm^{-1}). The yield of Glu232Asp was ~3 mg of protein/g wet cell.

Steady-State Kinetics. The initial velocity of the dehalogenase-catalyzed conversion of 4-CBA-CoA to 4-HBA-CoA was measured by monitoring the increase in solution absorption at 300 nm ($\Delta\epsilon$ = 8200 M^{-1} cm^{-1}) (*22*). The initial velocity data were analyzed using eq 1 and the computer program KinetAsyst (IntelliKinetics) to calculate V_m and K_m. The k_{cat} was calculated from the ratio of V_m and enzyme concentration:

$$V = V_{max}[S]/([S] + K_m) \quad (1)$$

where V is initial velocity, V_{max} maximum velocity, [S] the substrate concentration, and K_m the Michaelis constant.

Because of the low activity of the E232D dehalogenase K_m was not determined. The k_{cat} was calculated from the initial velocity measured at a saturating level of substrate. The initial velocity was determined by measuring the amount of 4-HBA-CoA (at 330 nm $\Delta\epsilon$ = 18200 M^{-1} cm^{-1} for the 4-HBA-CoA phenoxide anion) formed in reaction mixtures

incubated for a specific time period and then quenched with base (110 μL of 0.3 M KOH added to 110 μL of reaction mixture). Reactions were carried out in 50 mM K^+Hepes (pH 7.5 and 25 °C), which contained 20 μM E232D and 200 μM or 500 μM 4-CBA-CoA. The initial velocity of the reaction was calculated from the slope of a plot of product concentration vs reaction time.

Single-Turnover Reaction of the Wild-Type Dehalogenase Monitored by Stopped-Flow Absorption. The k_{obs} value for wild-type dehalogenase was measured using the published stopped-flow absorption method (*22*). The reaction mixture initially contained 45 μM enzyme and 15 μM 4-CBA-CoA in 50 mM K^+Hepes buffer (pH 7.5) at 25 °C. The progress of the reaction was monitored at 375 nm.

Single-Turnover Reaction of the E232D Dehalogenase Monitored by UV Absorption. The reaction of 45 μM Glu232Asp with 15 μM 4-CBA-CoA was carried out in 1 mL 50 mM K^+Hepes buffer (pH 7.5) at 25 °C. The 375 nm absorption of the reaction was monitored using a Beckman DU640 UV/visible spectrophotometer. The data were fitted to a single-exponential equation (eq 2) to obtain the observed rate constant k_{obs}:

$$A_t = A_{max}[1 - \exp(-tk_{obs})] \quad (2)$$

where A_t is the absorbance at a specific time t, A_{max} the maximal absorbance, and k_{obs} the apparent first-order rate constant.

Ligand Dissociation Constants Measured by Fluorescence Titration. The binding constants (K_d values) of the substrate analogue 4-methylbenzoyl-CoA (4-MBA-CoA) and the product 4-HBA-CoA with wild-type and mutant Glu232Asp dehalogenase were determined using the published procedure (*22*).

Single-Turnover Reactions Measured by Rapid Quench or Hand Quench. Time courses for the intermediate (EAr) and the product (EP + P) in the single-turnover reactions catalyzed by wild-type dehalogenase and the Glu232Asp mutant were determined by rapid quench (for wild type) or hand quench (for Glu232Asp mutant) according to the published procedure (*22*). Reaction solutions contained 100 μM dehalogenase and 50 μM 4-CBA-CoA in 1 mL of 50 mM K^+Hepes (pH 7.5) at 25 °C.

UV/Visible Difference Spectral Analysis of 4-HBA-CoA and 4-MBA-CoA Complexes Formed with Wild-Type and E232D 4-CBA-CoA Dehalogenase. UV/visible difference spectra were measured at 25 °C as previously described (*22*) using 1 mL quartz tandem cells containing 250 μL of 48 μM enzyme (wild type or E232D mutant) in 50 mM K^+-Hepes (pH 7.5) in one compartment and 250 μL of 200 μM 4-HBA-CoA or 4-MBA-CoA in 50 mM K^+Hepes (pH 7.5) in the other. The spectra measured before and after mixing the contents of the two compartments were subtracted to yield the difference spectrum.

COMPUTATIONAL METHODS

QM/MM calculations were performed for the wild-type and mutant enzyme−substrate complexes using CHARMM (*31*). The basic methods are described in detail in our previous work (*32*). Briefly, the initial coordinates of the wild-type ES complex were obtained from the crystal structure of the enzyme−product complex (Protein Data Bank code 1NZY) by replacing the hydroxyl group in the 4-HBA-CoA substrate with chlorine. Two adjacent subunits were included. The structures of the E232Q and E232D mutants were prepared by replacing Glu232 with either Gln or Asp. These structures were repeatedly solvated by preequilibrated TIP3P water (*33*) spheres, and stochastic boundary conditions (*34*) were imposed. The QM region consists of 25 atoms in the Asp145 side chain and the benzoyl group of the 4-CBA-CoA substrate and was treated with the semiempirical PM3 method (*35*). This choice of the QM treatment was based on earlier work that demonstrated that the PM3 results in this system follow closely with those obtained at the B3LYP/6-31+G(d,p) level (*36*). The QM/MM boundary atoms, namely, C_α of Asp145 and C_β of the mercaptoethylamine part of the CoA, were treated using the generalized hybrid orbital (GHO) method (*37*) with standard van der Waals parameters of the CHARMM22 force field. To mimic the solvent screening effect on charged residues, a charge-scaling approach (*38*) based on a classical Poisson−Boltzmann model was used for charged residues on the periphery of the protein.

The reaction path was first obtained along the putative reaction coordinate by adiabatic mapping, in which all coordinates except the reaction coordinate were optimized to minimize the total energy. For the S_NAr reaction, the reaction coordinate was defined as $R_\phi = R_{BC4-Cl} - R_{OD1-BC4}$. The configurations generated in a R_ϕ grid were later used as initial conditions in the PMF calculations. In the potential of mean force (PMF) simulations, the system at each window was first equilibrated for 50 ps, followed by data collection for an additional 50 ps.

To identify key residues in the wild-type enzyme that have significant electrostatic contributions to the catalysis, a charge perturbation method was used (*39*). The object is to determine the energy difference when the side chain charge of a residue is scaled to zero. The energy difference is defined as

$$\Delta\Delta E = \Delta E_{TS} - \Delta E_{ES} \quad (3)$$

with $\Delta E_{TS} = \Delta E_{TS}^{scale} - \Delta E_{TS}^{nonscale}$ and $\Delta E_{ES} = \Delta E_{ES}^{scale} - \Delta E_{ES}^{nonscale}$. Hence, a negative $\Delta\Delta E$ corresponds to stabilization of the transition state or destabilization of the reactant when the charge is zeroed.

The PMF for the catalyzed S_NAr reaction was determined by umbrella sampling (*40*) along the reaction coordinate R_ϕ. To facilitate efficient sampling, the reaction coordinate was constrained with harmonic biasing potentials in several windows. The final PMF was obtained using the weighted histogram analysis method (WHAM) (*41*).

RESULTS

Charge Perturbation Study of Wild-Type Dehalogenase. Our previous computational studies have indicated that the addition of the nucleophile (Asp145) to the C(4) of the substrate (4-CBA-CoA) is the rate-limiting step in the S_NAr reaction catalyzed by 4-CBA-CoA dehalogenase (*27*, *32*, *42*). To analyze the electrostatic influence of each residue in the wild-type enzyme on catalysis of this step, the energy contribution was computed for both the ground state and the EMc-forming transition state using the charge perturbation method (*39*). The energy difference as defined by eq 3 is

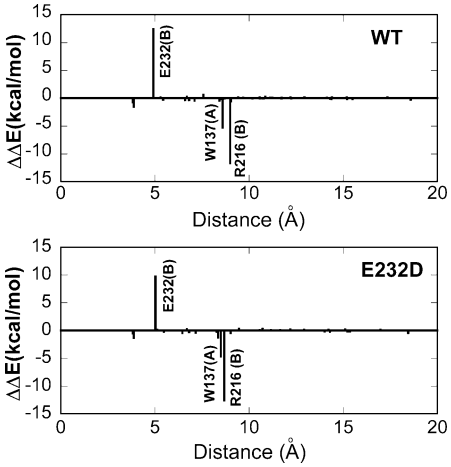

FIGURE 2: Graphical representation of the results for the WT enzyme (upper panel) and E232D mutant (lower panel) derived from the perturbation analysis of energy contributions from residues in the wild-type 4-CBA-CoA dehalogenase (see text for details). The energy difference as defined by eq 3 is plotted as a function of the $C_\alpha-C_\alpha$ distance to the nucleophile (Asp145). Positive values indicate favorable contributions that stabilize the rate-limiting transition state.

plotted in the upper panel of Figure 2 as a function of the $C_\alpha-C_\alpha$ distance to the nucleophile (Asp145). Although the energy difference is not expected to be quantitatively accurate, it serves as an indicator for residues that might engage in significant electrostatic interactions with the reactant as it proceeds along the reaction coordinate. It is apparent from this computation that Glu232(B), Arg216(B), and Trp137 make the largest electrostatic contributions. Trp137 engages in hydrogen bond interaction with the Asp145 (Figure 1B), and it has been previously shown to be an important component of the catalytic machinery (*26*, *27*, *32*). Glu232(B) and Arg216(B), on the other hand, are located at some distance from the catalytic site. Nevertheless, these residues are stringently conserved among the 4-CBA-CoA dehalogenase sequences. The C_γs of Glu232(B) and Arg216(B) which are 8.3 and 13.0 Å away from the benzoyl C(4), respectively (*24*), form a nearly straight line with the Asp145 nucleophile (Figure 3A). This alignment of charged residues suggests that a macrodipole formed by these two point charges might facilitate catalysis via interaction with Asp145.

Binding of 4-MBA-CoA and 4-HBA-CoA to E232D Dehalogenase. To test the contributions of the Glu232 and Arg216 residues to dehalogenase catalysis, these amino acids were mutated. Of the mutants prepared (E232D, E232A, E232Q, E232N, E232R, R216L, R216K, R216E, E232Q/R216L, and E232R/R216E) only E232D was expressed as a soluble protein. No attempt was made to optimize the expression of the soluble protein from the mutant genes, and we know from previous experience with a large number of dehalogenase active site mutants prepared in our laboratory that amino acid substitution in this enzyme frequently leads to insolubility. In the present case, we note that Glu232 and Arg216 are at the subunit interface and that these residues might contribute to subunit−subunit association. As illustrated in Figure 2B, Glu232(B) forms three hydrogen bonds with the backbone amide groups of Ser149 and Ala147 and with the side chain of Ser149, respectively. In addition, Arg216(B) forms two hydrogens bonds with Gln223(B) and

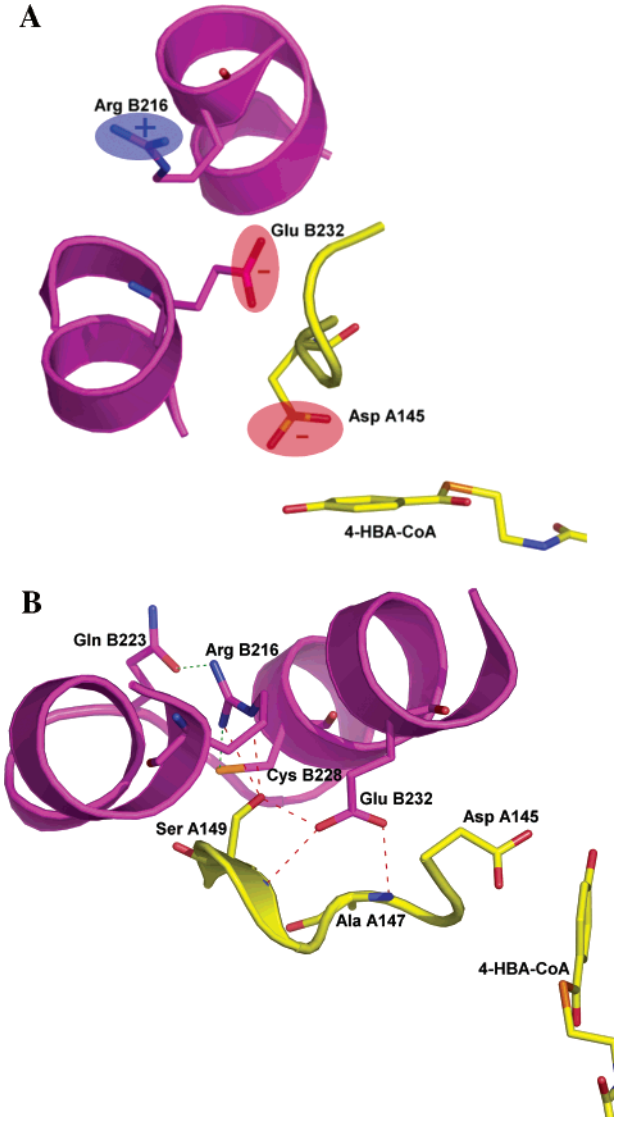

FIGURE 3: (A) Depiction of the alignment of point charges from Glu232(B), Arg216(B), and Asp145(A) generated from the coordinates of the X-ray structure of the wild-type 4-CBA-CoA dehalohenase−4-HBA-CoA complex (*24*). (B) Polar residues located at the subunit A−subunit B interface. Subunit B is colored magenta and subunit A yellow. Dashed lines signify hydrogen bonds.

Cys228(B), respectively. Amino acid substitution that destroys this hydrogen bond network might impact on solubility, which could explain why only the substitution of the Glu232 with Asp resulted in a soluble mutant enzyme.

The binding of 4-CBA-CoA substrate (and equally, the substrate analogue 4-MBA-CoA) and 4-HBA-CoA product ligands to the dehalogenase active site causes a substantial reduction in the intrinsic protein fluorescence (*21*, *22*). By monitoring the protein fluorescence as a function of ligand concentration at fixed dehalogenase concentration, the ligand binding curve can be measured, and from it the dissociation constant for the enzyme−ligand complex can be calculated. The K_d values for the E232D dehalogenase complexes of the substrate analogue 4-MBA-CoA and the product 4-HBA-CoA determined in this manner are compared with those measured for the wild-type dehalogenase in Table 1. The 4-MBA-CoA ligand offers the advantage that it does not undergo catalytic turnover, and it has been shown in previous studies (*14*) to be a reliable measure of the binding affinity

Table 1: K_d Values for Wild-Type and E232D 4-CBA-CoA Dehalogenase Complexes of 4-HBA-CoA and 4-MBA-CoA Measured in 50 mM K^+Hepes (pH 7.5, 25 °C)

	K_d (μM)	
ligand	wild-type dehalogenase	E232D dehalogenase
4-MBA-CoA	1.6 ± 0.2	0.06 ± 0.06
4-HBA-CoA	0.6 ± 0.2	0.19 ± 0.09

of the 4-CBA-CoA. Overall, the ligand binding is tighter with the mutant, especially in the case of the 4-MBA-CoA where the K_d decreases by at least an order of magnitude. We note, however, that as the binding affinity increases to a K_d value below 1 μM, the K_d value derived from the ligand titration curve becomes less well defined (for discussion of this limitation see ref *14*). Although we are certain that ligand binding is significantly tighter in the mutant, it would not be prudent to assign an exact numerical value to this increase.

The enhanced ligand binding has two important implications. First, it is strong evidence that the active site is intact and thus that the mutation has not disrupted the native fold. Second, it indicates that the repositioning of the subunit B Glu232 point charge, located outside of the subunit A active site (Figure 3A), influences the electrostatic environment of the substrate binding site.

Catalytic Activity of the E232D Dehalogenase. The catalytic activity of E232D dehalogenase was first examined under multiple-turnover conditions. The rates of product formation from the reactions of 200 μM enzyme and with 500 μM 4-CBA-CoA were shown to be equivalent, which demonstrates that the enzyme was saturated with substrate, and therefore that the initial velocity measured approximates the maximum velocity. Accordingly, the k_{cat} for E232D dehalogenase is 1.5×10^{-4} s^{-1} compared to 0.6 s^{-1} measured for the wild-type enzyme (Table 2). The single-turnover rate for wild-type dehalogenase is 2.3 s^{-1}, ~4-fold faster that the multiple-turnover rate (*22*). The single-turnover rate measured for the E232D mutant is $(2.16 \pm 0.02) \times 10^{-4}$ s^{-1}, which is essentially the same as the multiple-turnover rate. Thus, for the mutant, a chemical step is rate limiting, and it is 10000-fold slower than the rate-limiting chemical step catalyzed by the wild-type enzyme. According to transition state theory (eq 4), this reduction in k_{obs} corresponds to a 5.6 kcal/mol increase in the energy barrier for the enzymatic reaction:

$$k = \frac{k_B T}{h} \exp(-\Delta G^{\ddagger}/RT) \quad (4)$$

where k_B, h, and R are Boltzmann, Planck, and gas constants, respectively, and $\Delta G^{\ddagger}$ is the activation free energy. The transmission constant is assumed to be unity, and $T = 300$ K.

Evaluation of the Accumulation of the EAr Intermediate in the Glu232Asp Dehalogenase Catalysis. The observed rate constant for the single-turnover reaction (k_{obs}), reported in the previous section, is the culmination of the microscopic rate constants governing both partial reactions (Scheme 1). In the wild-type dehalogenase, the efficiency of the two partial reactions is roughly balanced, and as a result the EAr intermediate accumulates during the single-turnover reaction to 22% of the bound substrate (Figure 4A). In contrast, with the E232D mutant EAr accumulation was not detected (Figure 4B). The $k_{obs} = (2.16 \pm 0.02) \times 10^{-4}$ s^{-1} thus reflects the apparent rate constant for the first partial reaction. Accordingly, the 5.6 kcal/mol increase in the energy barrier can be attributed to the rate-limiting step of the S_NAr partial

Table 2: Steady-State (k_{cat} and K_m) and Single-Turnover (k_{obs}) Rate Constants Measured for Conversion of 4-CBA-CoA to 4-HBA-CoA Catalyzed by Wild-Type and E232D 4-CBA-CoA Dehalogenase in 50 mM K^+Hepes (pH 7.5, 25 °C)[a]

dehalogenase	k_{cat} (s^{-1})	k_{obs} (s^{-1})	K_M (μM)	$\Delta G^{\ddagger}_{exp}$ (kcal/mol)	$\Delta G^{\ddagger}_{theo}$ (kcal/mol)
wild type[b]	0.60 ± 0.01	2.3 ± 0.1	3.7 ± 0.3		
E232D	1.5×10^{-4}	$2.16 (\pm 0.02) \times 10^{-4}$	ND[c]	5.6	6.0

[a] The experimental ($\Delta G^{\ddagger}_{exp}$) free energy difference between the ES complex and the rate-limiting transition state was calculated from k_{obs} whereas the theoretical ($\Delta G^{\ddagger}_{theo}$) free energy difference was determined by the potential of mean force simulation of the S_NAr reaction coordinate. [b] Kinetic values are from ref *52*. [c] K_M was not determined because of the low activity of the E232D mutant.

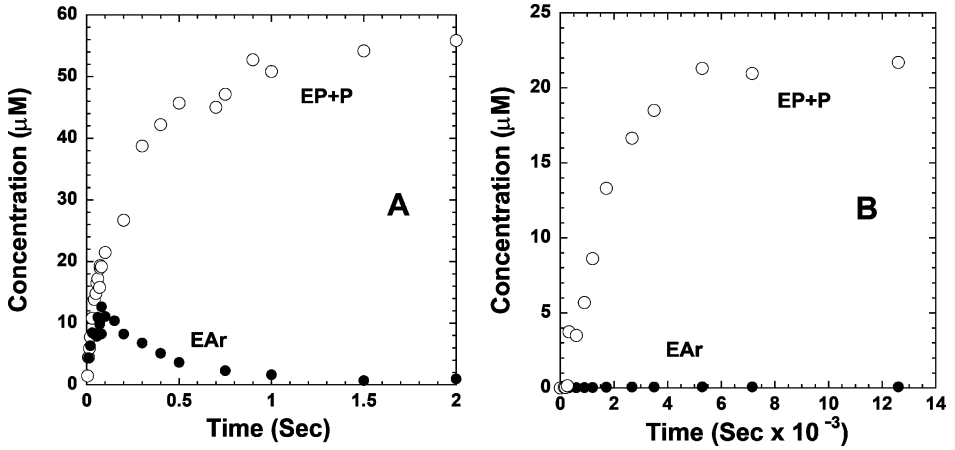

FIGURE 4: (A) Time course for a single-turnover reaction of 52 μM 4-CBA-CoA catalyzed by 115 μM wild-type 4-CBA-CoA dehalogenase at 25 °C in 50 mM K^+Hepes (pH 7.5) measured by rapid quench. (B) Time course for a single-turnover reaction of 50 μM 4-CBA-CoA catalyzed by 100 μM 4-CBA-CoA dehalogenase mutant E232D at 25 °C in 50 mM K^+Hepes (pH 7.5) measured by hand quench.

Table 3: Key Geometric Parameters between the Nucleophile and Substrate in the ES Complex Calculated from Minimal Energy Configurations

enzyme	$d_{OD1-BC4}$ (Å)	$d_{OD2-BC4}$ (Å)	$\theta_{OD1-BC4-BC3}$ (deg)	$\theta_{OD1-BC4-BC5}$ (deg)
wild type	3.22	3.04	85.0	79.6
E232D	3.03	3.29	89.8	85.9

reaction, which in the wild-type dehalogenase is the EMc-forming step (*32*).

Polarization of the Substrate. The dehalogenase active site environment induces reorganization in the benzoyl ring π-electrons of the substrate ligand 4-CBA-CoA (and equally in the substrate analogue ligand 4-MBA-CoA) (*14*). The perturbation in π-electrons has been observed using ^{13}C NMR, Raman difference, and UV difference as spectral probes) (*14*). As discussed earlier in the introduction, the reorganization in the benzoyl ring π-electrons results from the electron induction by the oxyanion hole operating of the benzoyl carbonyl and the electrostatic push from the Asp145 carboxylate operating on the ring C(4) (Figure 1B). The polarization of π-electrons appears to be enhanced by the aromatic residues encircling the benzoyl ring. In the UV difference spectrum (the spectrum of uncomplexed enzyme and ligand is subtracted from the spectrum of the enzyme−ligand complex) the polarization effect is manifested by a peak at 300 nm, which has been assigned to the red-shifted absorption band of the ligand benzoyl chromophore (normally at 260 nm) (*14*). The molar extinction coefficient associated with the 300 nm peak is 4.46 mM^{-1} cm^{-1} for the wild-type complex. The molar extinction coefficient derived for the 4-MBA-CoA complexed to a dehalogenase mutant is thought to be an indicator of the polarizing environment of its active site. The UV difference spectra for the 4-MBA-CoA complexes of the wild-type and E232D dehalogenase are shown in Figures 5A,B. The absorptivity of the mutant is ~30% of that of the wild-type dehalogenase.

This result is most easily understood in the context of the UV difference spectra measured for the respective dehalogenase complexes of 4-HBA-CoA. 4-HBA-CoA exhibits an especially long wavelength benzoyl absorption band (shifted from a λ_{max} at 292 nm with a shoulder at 335 nm to a λ_{max} at 375 nm) when bound to the dehalogenase active site owing to the contribution of the C(4)OH nonbonding electrons. The Asp145, which can form a hydrogen bond with the C(4)-OH, no doubt enhances the substituent effect. The enzyme conformer that gives rise to the ring polarization exists in rapid equilibrium with a second conformer, which does not induce this large shift; i.e., λ_{max} is at 330 nm (*14*). The ratio of the 375 and 330 nm absorptions is an indicator of the ratio of the two conformers. In Figure 5C,D, the UV difference spectra of the 4-HBA-CoA complexes of the wild-type and E232D dehalogenase are shown. The 375:330 nm absorption ratio is 3:1 for wild-type dehalogenase (12.84 vs 3.91 mM^{-1} cm^{-1}) and 1:4 for the E232D mutant (0.91 vs 3.97 mM^{-1} cm^{-1}). Thus, active site of the E232D dehalogenase appears to exert a diminished polarizing effect on the benzoyl ring than is observed for the wild-type enzyme.

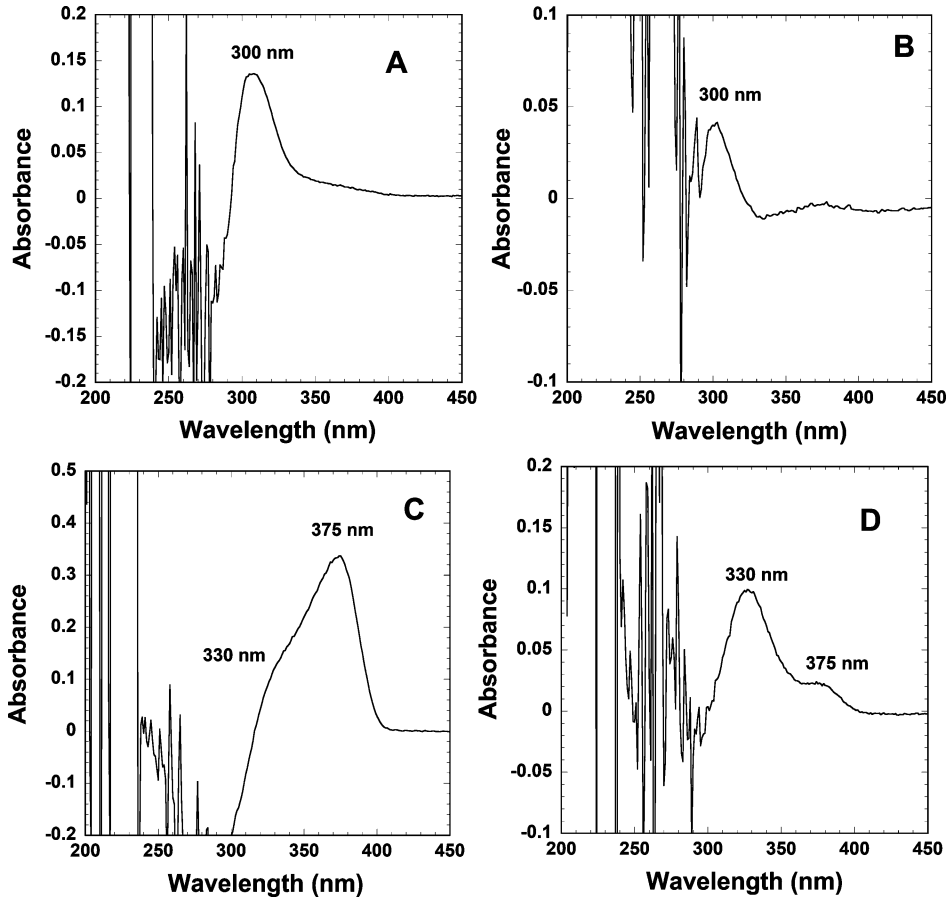

FIGURE 5: UV difference spectrum of 24 μM wild-type dehalogenase (A) or E232D dehalogenase (B) and 100 μM 4-HBA-CoA in 50 mM K^+Hepes (pH 7.5) at 25 °C. UV difference spectrum of 24 μM wild-type dehalogenase (C) or E232D dehalogenase (D) and 100 μM 4-MBA-CoA in 50 mM K^+Hepes (pH 7.5) at 25 °C.

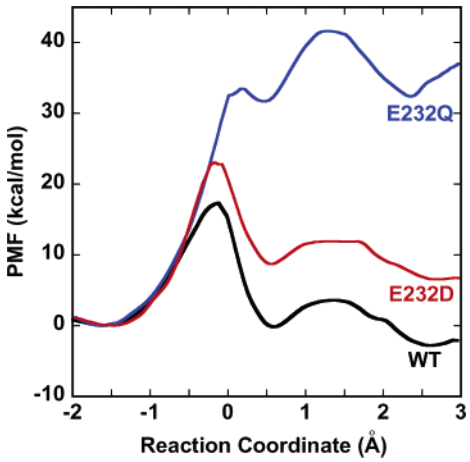

FIGURE 6: Comparison of the PMFs for the S_NAr reaction catalyzed by the wild-type, E232D, and E232Q 4-CBA-CoA dehalogenases. All PMFs are related to their corresponding ES energies, which are set to zero. See text for details.

Potentials of Mean Force for the E232D and E232Q Mutants. To provide insight into the energetics of the S_NAr reaction catalyzed by wild-type 4-CBA-CoA dehalogenase, we have computed the QM/MM PMFs along the putative reaction coordinate R_ϕ for the E232D and E232Q mutants. In calculating the PMFs, we divided the coordinate space into 27 separate windows and used a harmonic biasing potential in each window. The force constant of the biasing potential was mostly 50 kcal/(mol Å^2) but was increased to 100 kcal/(mol Å^2) near the barrier. The initial configuration for the MD simulation in each window was adopted from the minimal energy configuration determined by adiabatic mapping.

The PMFs for the mutants are compared in Figure 6 with that for the wild-type enzyme. The removal of the charge at position 232 by Gln substitution completely inactivates the enzyme, as evidenced by a large increase in the free energy barrier. A minor modification in the E232D mutant still results in a 23.1 kcal/mol free energy barrier for formation of EMc, which represents an increase of 6.0 kcal/mol relative to that of the wild-type enzyme. The increase of the free energy barrier is in good accord with the experimentally determined difference in k_{obs} values (~10000-fold) between the wild-type enzyme and the E232D mutant.

A comparison of the minimal energy enzyme−substrate (ES) structures of the wild-type 4-CBA-CoA dehalogenase and the E232D mutant bound with 4-CBA-CoA is made in Figure 7. Both structures show the Asp145 side chain in the NAC (*43*). However, whereas in the wild-type dehalogenase Glu232(B) carboxylate group is pointing at the Asp145 carboxylate group, in the mutant Asp232(B) is pointing away from it. The four distances between the respective carboxylate oxygen atoms are 6.13, 6.53, 7.37, and 7.57 Å for the mutant, which can be compared with 5.59, 5.95, 7.43, and 7.50 Å in the wild type. The larger distance between the carboxylate groups of Asp145 and Asp232(B), particularly the shortest O−O distance, leads to a reduced electrostatic interaction. Also, in the structure of the wild-type dehalogenase, the side chain of Glu232(B) forms three hydrogen bonds with the backbone amide groups of Ala147 and Ser149 and the hydroxyl group of the Ser149 side chain, respectively, but in the E232D mutant the removal of the methylene unit

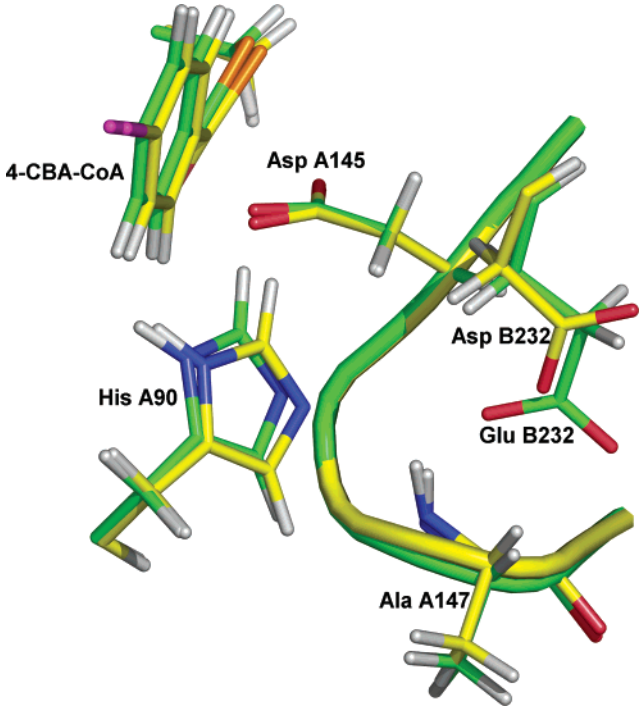

FIGURE 7: Comparison of the minimal energy ES structures of the active sites of wild-type 4-CBA-CoA dehalogenase (green) and the E232D mutant (cyan) bound with 4-CBA-CoA. See text for details.

disrupts the hydrogen bond between Ala147 and Asp232(B). In its place, a hydrogen bond is formed between the backbone amide group of Ala147 and the His90 side chain. The side chain His90 closes to a β-turn and forms another hydrogen bond to stabilize this β-turn. We note that the conformational changes in the E232D mutant derived from modeling have not been verified by structural data (owing to our failure to find suitable crystallization conditions for X-ray structure determination) and are therefore tentative. Nonetheless, the theoretical analysis provides insight into the potential effect of Glu232 located on subunit B, on catalysis taking place in the active site of subunit A, that currently is unobtainable by an experimental approach.

To ascertain that the electrostatic effect of residue 232 in the B subunit is responsible for the increased barrier in the E232D mutant, we have repeated the charge perturbation calculation for the reaction path of the mutant. As shown in the lower panel of Figure 2, the removal of the side chain charges of D232 in the mutant renders a smaller increase of the barrier height than that in the wild-type enzyme. This finding suggests that Asp232 of the D232 mutant exerts a weaker electrostatic interaction with the active site of the adjacent subunit than does the Glu232 of the wild-type dehalogenase.

DISCUSSION

In this work, we have shown using experimental methods that substitution of Glu232(B) with Asp enhances substrate binding, reduces substrate benzoyl ring polarization, and reduces the rate of catalytic turnover. On the basis of these observations we propose that the preorganized dipole formed by Arg216(B)−Glu232(B) (Figure 3A), located outside of the active site, affects substrate binding and catalysis occurring within the active site through its influence on the Asp145 nucleophile.

There are several different ways that Asp145 might be affected by the Arg216(B)−Glu232(B) dipole. First, it might influence the population and interconversion rates of Asp145 side chain rotomers. Although the simulation indicated that Asp145 in both wild-type and E232D dehalogenase assumes a near attack conformation, we know from the crystal structures that other rotomers exist (Figure 1C). Unfortunately, owing to the present limitations imposed on computational methodology, we cannot access the rotomer energies nor the energy barriers for rotomer interconversion in the wild-type or mutant enzymes.

Second, it is also possible that the mutation of E232(B) induces conformational change at the interface between the subunits, thus altering the electrostatic environment of the active site. This scenario should be detectable by X-ray structural determination of the mutant, but unfortunately our repeated attempts to crystallize the mutant enzyme were unsuccessful. Theoretically, such slow conformational changes would be difficult to observe in MD simulations on a nanosecond time scale, particularly when the entire protein is restrained by the stochastic boundary conditions used in this work.

Third, the Arg216(B)−Glu232(B) dipole might produce an unfavorable electrostatic interaction with the Asp145 in the ground state, which, because of charge dissipation in transition state, serves to reduce the energy barrier to the rate-limiting EMc-forming step. This is the scenario simulated by the theoretical model presented above. It is interesting to note that the model is, in effect, catalysis via ground state destabilization (GSD), which has been extensively debated in the literature (*44*−*50*). An important consequence of GSD is that there is increased substrate binding energy, along with the reduced catalytic activity, when the destabilization interaction is removed or weakened. In the extensively studied orotidine 5′-monophosphate decarboxylase (ODCase), the GSD model was initially argued but then later was dismissed (*48*) on the basis of experimental evidence which demonstrated a decreased binding energy for a substrate analogue which lacks the putative repulsive charged functional group (*49*). In the dehalogenase, however, the decreased K_d values determined for two substrate analogues in complex with the E232D mutant (Table 1) are consistent with the GSD model.

The fact that we do not have an X-ray structure of the E232D dehalogenase, which might serve to distinguish between these three scenarios presented, is indeed frustrating. Nonetheless, it is quite clear that a remote residue does make an important electrostatic contribution to the catalytic machinery of the 4-CBA-CoA dehalogenase. This is a significant finding because it is generally believed that enzyme catalysis is largely determined by the active site residues. As a result, mutation experiments involving residues far away from the active site are seldom attempted. However, there are several recent studies that have indicated that remote residues can have a significant impact on the catalysis in enzymes. For example, Cameron and Benkovic reported that a single mutation of Gly121 in dihydrofolate reductase 19 Å away from the active site can result in a 200-fold reduction of k_{cat} (*51*). Oelschlaeger et al. also found that a remote residue (Gly262) in an imipenemase (IMP-1) can have a significant effect on the substrate specificity of this metallo-β-lactamase. In ODCase, which is probably more relevant to the current system, mutations of active site residues that are ∼8 Å away from the bond cleavage site were found to have strong electrostatic contributions to the catalysis (*52*). To our best knowledge, however, this is the first time long-range electrostatic control of the catalysis by a remote and non active site residue has been identified in an enzymatic system. It serves to underscore the potential for a joint theory−experiment approach to enzymology.

SUMMARY

The paradigm for 4-CBA-CoA dehalogenase catalysis is based on the polarization of the benzoyl group by the enzymatic oxyanion hole acting on the carbonyl group, which stabilizes the negative charge brought about by the nucleophilic addition. The observation that the charge is transferred over five bonds also suggests that the catalysis may be highly susceptible to electrostatic control. Indeed, there has been ample experimental and theoretical evidence suggesting that perturbations of the oxyanion hole partially impair the catalysis. In this work, we provide further evidence that the catalytic scaffold also includes charged residues that are not part of the active site.

We have focused on Glu232 on the B subunit of the enzyme, which is the closest charged residue to the nucleophile in the adjacent subunit A. As suggested by a charge perturbation analysis along the reaction path of the wild-type enzyme, this charged residue seems to have an important role in lowering the rate-limiting barrier in the S_NAr reaction step. This is confirmed by both experimental site-directed mutagenesis studies and PMF calculations. Although attempts to substitute this residue with a noncharged residue were unsuccessful, a viable mutant (Glu232Asp) was prepared, and its kinetic properties were characterized to demonstrate a significant reduction of the catalytic efficiency. The increase of the free energy barrier is reproduced by the mutant PMF in a theoretical model. The combined experimental and theoretical results provide strong evidence that the Glu232(B) residue provides electrostatic forces that could act on the orientation of the Asp145 nucleophile as well to destabilize the ground state of the catalyzed S_NAr reaction. We suspect that the Glu232 point charge works in conjunction with other nearby charged residues, such as Arg216-(B), to modulate the electrostatic environment at the active site. However, existing experimental and theoretical data are insufficient to rule out other possibilities such as conformational changes of the enzyme.

REFERENCES

1. Dunaway-Mariano, D., and Babbitt, P. C. (1994) On the origins and functions of the enzymes of the 4-chlorobenzoate to 4-hydroxybenzoate converting pathway, *Biodegradation 5*, 259−276.
2. Loffler, F., Lingens, F., and Muller, R. (1995) Dehalogenation of 4-chlorobenzoate, *Biodegradation 6*, 203−212.
3. Commandeur, L. C. M., and Parsons, J. R. (1990) Degradation of halogenated aromatic compounds, *Biodegradation 1*, 207−220.
4. Abramowicz, D. A. (1990) Aerobic and anaerobic biodegradation of PCBs: a review, *Crit. Rev. Biotechnol. 10*, 241−248.
5. Scholten, J. D., Chang, K.-H., Babbitt, P. C., Charest, H., Sylvestre, M., and Dunaway-Mariano, D. (1991) Novel enzymic hydrolytic dehalogenation of a chlorinated aromatic, *Science 253*, 182−185.
6. Chang, K.-H., Liang, P. H., Beck, W., Scholten, J. D., and Dunaway-Mariano, D. (1992) Isolation and characterization of the three polypeptide components of 4-chlorobenzoate dehalogenase from *Pseudomonas* sp. strain CBS-3, *Biochemistry 31*, 5605−5610.

7. Liang, P.-H., Yang, G., and Dunaway-Mariano, D. (1993) Specificity of 4-chlorobenzoyl coenzyme A dehalogenase catalyzed dehalogenation of halogenated aromatics, *Biochemistry 32*, 12245−12250.
8. Crooks, G. P., and Copley, S. D. (1993) A surprising effect of leaving group on the nucleophilic aromatic substitution reaction catalyzed by 4-chlorobenzoyl-CoA dehalogenase, *J. Am. Chem. Soc. 115*, 6422−6423.
9. Yang, G., Liang, P.-H., and Dunaway-Mariano, D. (1994) Evidence for nucleophilic catalysis in the aromatic substitution reaction catalyzed by (4-chlorobenzoyl) coenzyme A dehalogenase, *Biochemistry 33*, 8527−8531.
10. Liu, R.-Q., Liang, P.-H., Scholten, J., and Dunaway-Mariano, D. (1995) Transient state kinetic analysis of the chemical intermediates formed in the enzymic dehalogenation of 4-chlorobenzoyl coenzyme A, *J. Am. Chem. Soc. 117*, 5003−5004.
11. Taylor, K. L., Liu, R.-Q., Liang, P.-H., Price, J., and Dunaway-Mariano, D. (1995) Evidence for electrophilic catalysis in the 4-chlorobenzoyl-CoA dehalogenase reaction: UV, Raman, and ^{13}C-NMR spectral studies of dehalogenase complexes of benzoyl-CoA adducts, *Biochemistry 34*, 13881−13888.
12. Crooks, G. P., Xu, L., Barkley, R. M., and Copley, S. D. (1995) Exploration of possible mechanisms for 4-chlorobenzoyl CoA dehalogenase: evidence for an aryl-enzyme intermediate, *J. Am. Chem. Soc. 117*, 10791−10798.
13. Yang, G., Liu, R.-Q., Taylor, K. L., Xiang, H., Price, J., and Dunaway-Mariano, D. (1996) Identification of active site residues essential to 4-chlorobenzoyl-coenzyme A dehalogenase catalysis by chemical modification and site directed mutagenesis, *Biochemistry 35*, 10879−10885.
14. Taylor, K. L., Xiang, H., Liu, R.-Q., Yang, G., and Dunaway-Mariano, D. (1997) Investigation of substrate activation by 4-chlorobenzoyl-coenzyme A dehalogenase, *Biochemistry 36*, 1349−1361.
15. Clarkson, J., Tonge, P. J., Taylor, K. L., Dunaway-Mariano, D., and Carey, P. R. (1997) Raman study of the polarizing forces promoting catalysis in 4-chlorobenzoate-CoA dehalogenase, *Biochemistry 36*, 10192−10199.
16. Dong, J., Xiang, H., Luo, L., Dunaway-Mariano, D., and Carey, P. R. (1999) Modulating electron density in the bound product, 4-hydroxybenzoyl-CoA, by mutations in 4-chlorobenzoyl-CoA dehalogenase near the 4-hydroxy group, *Biochemistry 38*, 4198−4206.
17. Xiang, H., Dong, J., Carey, P. R., and Dunaway-Mariano, D. (1999) Product catalyzes the deamidation of D145N dehalogenase to produce the wild-type enzyme, *Biochemistry 38*, 4207−4213.
18. Zhang, W., Wei, Y., Luo, L., Taylor, K. L., Yang, G., Dunaway-Mariano, D., Benning, M. M., and Holden, H. M. (2001) Histidine 90 function in 4-chlorobenzoyl-coenzyme A dehalogenase catalysis, *Biochemistry 40*, 13474−13482.
19. Luo, L., Taylor, K. L., Xiang, H., Wei, Y., Zhang, W., and Dunaway-Mariano, D. (2001) Role of active site binding interactions in 4-chlorobenzoyl-coenzyme A dehalogenase catalysis, *Biochemistry 40*, 15684−15692.
20. Lewandowicz, A., Rudzinski, J., Luo, L., Dunaway-Mariano, D., and Paneth, P. (2002) Determination of the chlorine kinetic isotope effect on the 4-chlorobenzoyl-CoA dehalogenase-catalyzed nucleophilic aromatic substitution, *Arch. Biochem. Biophys. 398*, 249−252.
21. Dong, J., Carey, P. R., Wei, Y., Luo, L., Lu, X., Liu, R.-Q., and Dunaway-Mariano, D. (2002) Raman evidence for Meisenheimer complex formation in the hydrolysis reactions of 4-fluorobenzoyl- and 4-nitrobenzoyl-coenzyme A catalyzed by 4-chlorobenzoyl-coenzyme A dehalogenase, *Biochemistry 41*, 7453−7463.
22. Dong, J., Lu, X., Wei, Y., Luo, L., Dunaway-Mariano, D., and Carey, P. R. (2003) The strength of dehalogenase-substrate hydrogen bonding correlates with the rate of Meisenheimer intermediate formation, *Biochemistry 42*, 9482−9490.
23. Miller, J. (1968) *Aromatic Nucleophilic Substitution*, Elsevier, Amsterdam.
24. Benning, M. M., Taylor, K. L., Liu, R.-Q., Yang, G., Xiang, H., Wesenberg, G., Dunaway-Mariano, D., and Holden, H. M. (1996) Structure of 4-chlorobenzoyl coenzyme A dehalogenase determined to 1.8 Å resolution: An enzyme catalyst generated via adaptive mutation, *Biochemistry 35*, 8103−8109.
25. Guo, H., and Salahub, D. R. (1998) Cooperative hydrogen bonding and enzyme catalysis, *Angew. Chem., Intl. Ed. 37*, 2985−2990.
26. Lau, E. Y., and Bruice, T. C. (2001) The active site dynamics of 4-chlorobenzoyl-CoA dehalogenase, *Proc. Natl. Acad. Sci. U.S.A. 98*, 9527−9532.
27. Xu, D., Guo, H., Gao, J., and Cui, Q. (2004) A QM/MM study of a nucleophilic aromatic substitution reaction catalyzed by 4-chlorobenzoyl-CoA dehalogenase, *Chem. Commun.*, 892−893.
28. Warshel, A., Aqvist, J., and Creighton, S. (1989) Enzymes work by solvation substitution rather than by desolvation, *Proc. Natl. Acad. Sci. U.S.A. 86*, 5820−5824.
29. Warshel, A. (1998) Electrostatic origin of the catalytic power of enzymes and the role of preorganized active sites, *J. Biol. Chem. 273*, 27035−27038.
30. Bradford, M. M. (1976) A rapid and sensitive method for the quantitation of microgram quantities of protein utilizing the principle of protein dye binding, *Anal. Biochem. 72*, 248−254.
31. Brooks, B. R., Bruccoleri, R. E., Olafson, B. D., States, D. J., Swaminathan, S., and Karplus, M. (1983) Charmm: A program for macromolecular energy, minimization, and dynamics calculations, *J. Comput. Chem. 4*, 187−217.
32. Xu, D., Wei, Y., Wu, J., Dunaway-Mariano, D., Guo, H., Cui, Q., and Gao, J. (2004) QM/MM studies of enzyme catalyzed dechlorination reaction of 4-chlorobenzoyl-CoA provide insight into reaction energetics, *J. Am. Chem. Soc. 126*, 13649−13658.
33. Jorgensen, W. L., Chandrasekhar, J., Madura, J. D., Impey, R. W., and Klein, M. L. (1983) Comparison of simple potential functions for simulating liquid water, *J. Chem. Phys. 79*, 926−935.
34. Brooks, C. L., III, and Karplus, M. (1983) Deformabal stochastic boundaries in molecular dynamics, *J. Chem. Phys. 79*, 6312−6325.
35. Stewart, J. J. P. (1989) Optimization of parameters for semiempirical methods. 1. method, *J. Comput. Chem. 10*, 209−220.
36. Zheng, Y.-J., and Bruice, T. C. (1997) On the dehalogenation mechanism of 4-chlorobenzoyl CoA by 4-chlorobenzoyl CoA dehalogenase: Insights from study based on the nonenzymatic reaction, *J. Am. Chem. Soc. 119*, 3868−3877.
37. Gao, J., Amara, P., Alhambra, C., and Field, M. J. (1998) A generalized hybrid orbital (GHO) method for the treatment of boundary atoms in combined QM/MM calculations, *J. Phys. Chem. A 102*, 4714−4721.
38. Simonson, T., Archontis, G., and Karplus, M. (1997) Continuum treatment of long-range interactions in free energy calculations. Application to protein−ligand binding, *J. Phys. Chem. B 101*, 8349−8362.
39. Bash, P. A., Field, M. J., Davenport, R. C., Petsko, G. A., Ringe, D., and Karplus, M. (1991) Computer simulation and analysis of the reaction pathway of triosephosphate isomerase, *Biochemistry 30*, 5826−5832.
40. Torrie, G. M., and Valleau, J. P. (1977) Non-physical sampling distributions in Monte Carlo free energy estimation: Umbrella sampling, *J. Comput. Phys. 23*, 187−199.
41. Kumar, S., Bouzida, D., Swendsen, R. H., Kollman, P. A., and Rosenberg, J. M. (1992) The weighted histogram analysis method for free energy calculations on biomolecules. 1. The method, *J. Comput. Chem. 13*, 1011−1021.
42. Xu, D., and Guo, H. (2005) Electrostatic influence of active-site waters on the nucleophilic aromatic substitution catalyzed by 4-chlorobenzoyl-CoA dehalogenase, *FEBS Lett. 579*, 4249.
43. Bruice, T. C., and Lightstone, F. C. (1999) Ground state and transition state contributions to the rates of intramolecular and enzymatic reactions, *Acc. Chem. Res. 32*, 127−136.
44. Jencks, W. P. (1975) Binding-energy, specificity, and enzymic catalysis—Circe effect, *Adv. Enzymol. Relat. Areas Mol. Biol. 43*, 219−410.
45. Fersht, A. R. (1999) *Enzyme Structure and Mechanism in Protein Science*, Freeman, New York.
46. Wu, N., Mo, Y., Gao, J., and Pai, E. F. (2000) Electrostatic stress in catalysis: structure and mechanism of the enzyme orotidine monophosphate decarboxylase, *Proc. Natl. Acad. Sci. U.S.A. 97*, 2017−2022.
47. Warshel, A., and Florian, J. (1998) Computer simulations of enzyme catalysis: Finding out what has been optimized by evolution, *Proc. Natl. Acad. Sci. U.S.A. 95*, 5950−5955.
48. Warshel, A., Strajbl, M., Villa, J., and Florian, J. (2000) Remarkable rate enhancement of orotidine 5′-monophosphate decarboxylase is due to transition-state stabilization rather than ground state destabilization, *Biochemistry 39*, 14728−14738.
49. Miller, B. G., Butterfoss, G. L., Short, S. A., and Wolfenden, R. (2001) Role of enzyme-ribofuranosyl contacts in the ground state

and transition state for orotidine 5′-phosphate decarboxylase: A role for substrate destabilization?, *Biochemistry 40*, 6227−6232.
50. Gao, J. (2003) Catalysis by enzyme conformational change as illustrated by orotidine 5′-monophosphate decarboylase, *Curr. Opin. Struct. Biol. 13*, 184−192.
51. Cameron, C. E., and Benkovic, S. J. (1997) Evidence for a functional role of the dynamics of glycine-121 of *Escherichia coli* dihydrofolate reductase obtained from kinetic analysis of a site-directed mutant, *Biochemistry 36*, 15792−15800.
52. Miller, B. G., Snider, M. J., Short, S. A., and Wolfenden, R. (2000) Contribution of enzyme-phosphoribosyl contacts to catalysis by orotidine 5′-phosphate decarboxylase, *Biochemistry 39*, 8113−8118.

BI051477W